

https://africanjournalofbiomedicalresearch.com/index.php/AJBR

Afr. J. Biomed. Res. Vol. 28(3s) (2025); 773-783

Research Article

Impact of Airflow and Particle Transport in Emphysema within Human Lungs via the Terminal Alveolated Duct

N.T. Mim¹, Muhammad Sajjad Hossain^{1*}, M. S. I. Mallik¹, M. Masum Billah¹, S.M.C. Hossain²

¹Department of Arts and Sciences, Ahsanullah University of Science and Technology (AUST), Dhaka-1208, Bangladesh

²Department of Applied Mathematics, University of Dhaka, Dhaka-1000, Bangladesh

*Corresponding author: Muhammad Sajjad Hossain *Email: msh.as@aust.edu, msh80edu@gmail.com

Abstract

Emphysema is the most common respiratory disease. Alveoli are the lung's smallest structures for gas exchange, where aerosol particle movement and deposition depend on convective airflow patterns. The geometrical model of emphysema is a space-filling single acinar region connected to a bronchiole. Particle deposition along with air flow changes due to the change of the structure of the alveolar sac for emphysema patients. The model consists of an elastic spherical cap (alveolus) attached to a rigid rectangular tube (bronchiole). This study investigates fluid flow and particle transport with the help of a computational fluid dynamic (CFD) model for the case of emphysema. This study is used to explore airflow patterns, fluid mixing, and particle deposition behaviour under controlled conditions, providing valuable insights into respiratory mechanics and aerosol transport in the lungs of emphysema patients.

Keywords: CFD, Airflow and particle transport, Emphysema, Alveolated duct, Finite Element method

Received -17/09/2024

Accepted-28/12/2024

DOI: https://doi.org/10.53555/AJBR.v28i3S.8077

© 2024 The Author(s).

This article has been published under the terms of Creative Commons Attribution-Noncommercial 4.0 International License (CC BY-NC 4.0), which permits noncommercial unrestricted use, distribution, and reproduction in any medium, provided that the following statement is provided. "This article has been published in the African Journal of Biomedical Research"

Introduction

Airflow and particle deposition are two mechanisms in the respiratory system that are closely associated. Breathing-induced airflow patterns alter how inhaled particles travel and finally deposit on the airway surfaces. Particle size, breathing rate, and airway shape all have some impact on where particles settle. The investigation of airflow and deposition of particles throughout simply one alveolar sac is critical to comprehending respiratory mechanics and the implications of airborne pollutants on the health of humans. The smallest functional units in the lungs are Alveoli where gas exchange occurs, and their performance can significantly impact overall

respiratory efficiency [1]. The motions of airflow and the deposition of inhaled particles in these structures are of significance in clinical studies, environmental science, and particle technology. Airflow contained by the alveolar sac is complex, with axial flow down the alveolar duct and collateral airflow into and out of individual alveoli. This complicated flow is regulated by the movement of alveolar walls and the presence of Kohn pores, which allow pressure to be equalized between adjacent alveoli. Airway shape, breathing habits, and lung elasticity all have an impact on airflow within the alveolar sac [2-3]. During breathes, air travels through increasingly narrower airways until it reaches the alveoli. The air movement in these sacs is characterized by low velocities and Reynolds numbers;

therefore it tends to be laminar rather than turbulent. [4]. The interaction among airflow along with the alveolar walls is crucial in optimizing the exchange of gas and preserving lung health. [5-7].

The deposition of particles in the alveoli is a key factor in respiratory health, particularly regarding the effects of pollutants, allergens, and pathogens. Particles inhaled into the respiratory system can vary greatly in size, composition, and behavior. Large particles are typically trapped in the upper respiratory tract, while smaller particles can reach the alveoli Understanding the mechanisms of particle deposition involves analyzing factors such as particle size, airflow patterns, and the biological and physical properties of the alveolar sac. Weibel [9] provides a detailed look at the geometric and morphometric characteristics of the lung's alveolar and bronchiolar Understanding the structure is crucial for studying how airflow behaves as it moves through these airways structures. Sznitman [10], Sznitman et al. [11], and Sutter et al. [12] had discussed the geometric complexity of the alveolar region and how it affects airflow patterns. The study emphasizes the transition from larger airways to the fine structure of alveolar sacs and its impact on laminar flow characteristics. Reis et al. [13], Xi et al. [14] provides a comprehensive review of respiratory flow and transport phenomena. It covers topics such as nasal airflow, gas transport in airways, alternative ventilation methods, aerosol dynamics, airway stability, mucus movement, pulmonary acoustics, surfactant behavior, and pleural fluid flow in human airway. Sul et al. [15] numerically investigated inspiratory and expiratory airflow in tracheobronchial airway models, highlighting how airflow velocity, pressure, and wall shear stress vary in normal and obstructed human airway. The findings contribute to understanding respiratory airflow characteristics and can inform treatments respiratory disorders.

Furthermore the use of computational fluid dynamics (CFD) and particle tracking methods to simulate particle deposition in the alveolar region of the lungs is explored by the several researchers [16-17]. Their study provided valuable insights into how different particle sizes and flow conditions influence deposition patterns. By employing CFD, they were able to model airflow and particle transport dynamics, which are crucial for understanding respiratory drug delivery, pollutant exposure, and inhalation toxicology. Kumar et al. [18] employs a three-dimensional honeycomblike model to represent alveolar ducts and sacs, analyzing how geometric features affect airflow patterns within the acinar region. The findings highlight that variations in alveolar geometry can lead to differences in flow behavior, which in turn influence particle transport and deposition. Also, aerosol particle transport and deposition in the intra-acinar region under various breathing scenarios is simulated by some researchers [19-20]. The study underscores the significance of alveolar geometry and wall motion in determining particle trajectories and deposition. Hofemeier and Sznitman [21-23] present an experimental model of acinar structures with moving

walls to capture breathing-like motions. This study provides insights into how realistic acinar geometries and dynamics influence particle transport and deposition patterns. Francis and Saha [24] examine the impact of surface tension on airflow behavior and alveolar mechanics, emphasizing the role of surfactant layers in maintaining normal respiratory function. Kumar et al. [25] investigate the role of asymmetry in alveolar wall motion on particle transport, providing evidence of chaotic mixing in the alveolar region, which has implications for particle deposition and respiratory health. These studies collectively enhance our understanding of how acinar geometry influences airflow dynamics and particle behavior, which is crucial for improving pulmonary drug delivery and assessing inhalation risks. An acinar unit is about 8 mm in diameter, contains up to 10,000 alveoli with each alveolus having the diameter 2–3 times smaller than the pencil head [26]. The diameter of the alveoli may vary significantly, for example, from 0.46 mm to 0.89 mm in COPD patients and from 0.2 mm to 0.45 mm in healthy subjects [27-29]. The size of alveoli can also change in diseased lungs. For instance, in emphysema, the septal walls (elastin) breaks down partially or completely due to the dissolution of inflammatory chemicals, leading to large airspaces and reduced recoil [30-31]. Lung tumors can compress the alveoli and reduce gas exchange capacity [32]. In some cases, the tumor will fill the alveoli. In cavitary pulmonary pneumonia [33], alveoli can become enlarged by bacterial infection, fungal infection, vasculitis, collagen vascular diseases, or sarcoidosis. In pulmonary edema, fluids accumulate in the alveoli, reducing its airspace and gas exchange area [34]. The alveolar size how affects the behavior and fate of inhaled aerosols is not still fully clear. Although it is generally acknowledged that smaller alveoli have a higher retention rate of inhaled aerosols, the mechanisms underlying particle behaviors in the acinar region are arguably the most diverse in the entire respiratory tract. Gravitational sedimentation dictates the deposition for large particles (>2.0 µm), Brownian motion influences ultrafine particles (<0.1um) while chaotic mixing determines fine aerosols $(0.1-2 \mu m)$ [21,22]. Therefore, the process and distributions of deposition are more complex than those predicted using the compartment model that assumed uniform particle deposition within each compartment. This research presents a novel combination of a subject-specific multi-scale airflow model and its effect on particle deposition. The airflow and particle deposition in the airways were solved under unsteady breathing conditions, and the CFD model was used to predict the influence on deposition and distribution of particles in the conducting airways of the lung [35].

To the finest understanding of scientists, the study of airflow and particle deposition in single alveolar sacs in emphysema is fundamental to comprehending lung function and health impacts. Research in this field spans experimental, theoretical, and computational approaches to understand how airflow patterns affect particles deposit in alveoli for emphysema. Advances in imaging and modeling technologies continue to

enhance our ability to study these phenomena, providing valuable insights into respiratory health and the effects of environmental exposures.

Description of the geometrical configuration

For simplicity we have used a 2D cross section of alveolar sac [36]. The geometry is constructed with four interconnected cluster of alveolus which is connected to respiratory bronchioles via alveolar ducts (See Figure 1). These ducts should be modeled to accurately represent the inlet and outlet for airflow into

and out of the alveolar sac. Briefly, the duct is modeled as a cylindrical shell with open ends, defined by a length $d=0.556~\mathrm{mm}$ and a diameter $Dd=0.286~\mathrm{mm}$. The spherical alveolus is of the radius $0.2\mathrm{mm}$ [9]. Pulmonary alveoli are closely arranged, hollow polyhedral structures that share common boundary walls, known as interalveolar septa. These alveoli are arranged in a manner similar to honeycombs or soap foams. We define five cut lines at different positions in the diagram for our further research purpose.

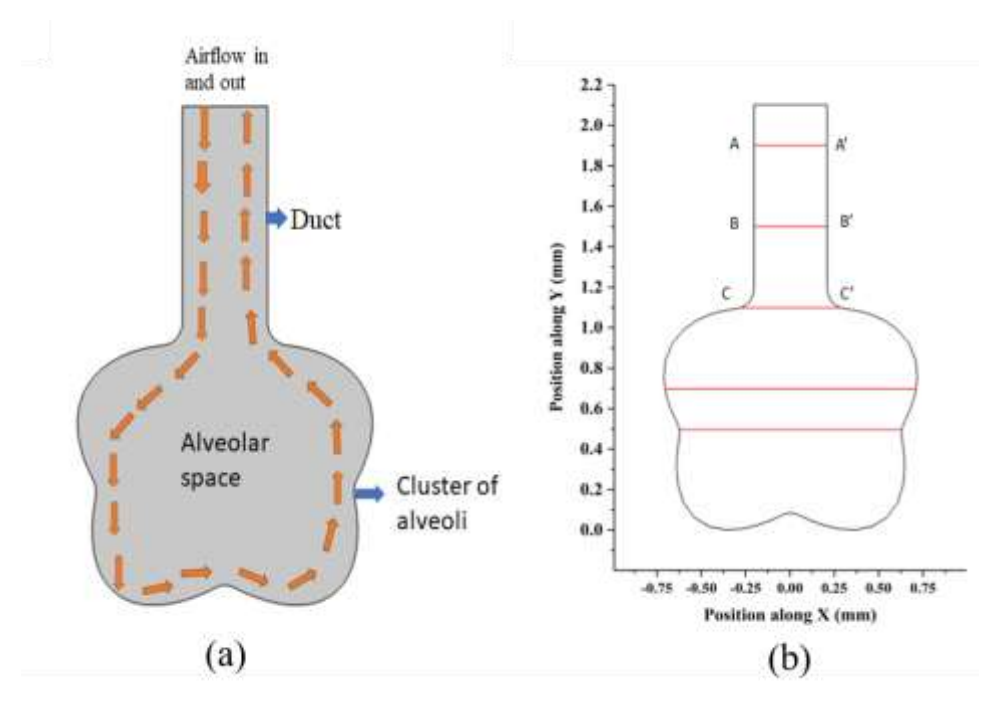


Figure 1: (a) 2D geometry of single alveolar sac (b) Geometry with different cut lines

Governing equations

Since the muck number is very low. The governing equation of the incompressible steady air [14] is

Continuity:
$$\frac{\partial u}{\partial t} + \nabla \cdot u = 0$$
 (1)

Momentum:
$$\rho \left(\frac{\partial u}{\partial t} + u \cdot \nabla u \right) = -\nabla P + \mu \nabla^2 u$$
 (2)

The primary mechanism for deposition in the alveoli and smaller airways is Brownian diffusion. The upper airway also serves as a filter for particles as small as 0.001m. Deposition of particles of sizes between 1 and 10 µm is primarily caused by inertial impaction and gravitational sedimentation. The trajectory equation can be expressed as follows if drag and gravity are assumed to be the most important forces on the particles along with Brownian and Lift force [14]:

$$\frac{dx}{dt} = u \tag{3}$$

$$\frac{du}{dt} = f_D(u - u_p) + g(1 - \alpha) + f_B + f_L \tag{4}$$

Where x, the position of the particles; g , acceleration due to gravity; α denotes the ratio. $\alpha = \frac{\rho}{\rho_p}$ and

 f_D The drag force coefficient of per unit particle mass. Here f_B , f_L are Brownian and Lift forces respectively.

Boundary Conditions: Uniform velocity profiles were applied at the inlet crosssection. Pressure-outlet boundary condition was adopted at the outlets. Nonslip boundary condition was employed along the airway walls. In order to complete the particle transport formulations, the uniform inlet particle profile, was adopted with the initial velocity of the corresponding airflow velocity. For all the walls, the trap condition was applied with the assumption that particles were trapped as soon as they touch the wall surfaces. Escape condition was applied to the inlets.

Particle deposition: Particle deposition fraction in the alveolus is calculated by the ratio of particle entering

into the lungs to the particle deposited into the region. Mathematical formula is:

 $DF = \frac{\text{Number of particle deposited into the egion}}{\text{Number of particle entering into the region}}$

Solution technique

The Galerkin weighted residual approach (GWRA) of finite element technique has been used to solve the non-dimensional main partial differential equations e.g. the continuity and Navier-Stokes equations using appropriate boundary conditions. Dechaumphai [37], Taylor and Hood [38], and Reddy [39] provide a thorough explanation of this method. This method involves discretizing the solution domain into finite element meshes and then using GWRA to find a system of integral equations from non-linear governing equations. To complete the integration involved in each expression of these equations, the Gauss quadrature method is used. Boundary conditions have then been applied to modify non-linear algebraic equations. Newton's technique is then used to relocate these modified equations into linear algebraic equations.

Lastly, the triangular factorization procedure is used to solve these linear equations. The PDE solver COMSOL Multiphysics and MATLAB programing are used to adapt the technique. The following criteria of equation (5) [40] are used to ensure the convergence of the algorithm for all dependent variables in domain Ω ,

$$\left| \varphi_{ii}^{n} - \varphi_{ii}^{n-1} \right| \le 10^{-5} \tag{5}$$

Where, φ denotes a velocity, pressure and stress tensor variable u, ρ , σ correspondingly and i, j implies a nodal point of elements; and the number of iterations is n at the grid level.

Grid independence test with model validation

The minimal number of elements required in the model to ensure that the mesh size does not impact the study outcomes is established by the grid independence test. Once a certain amount of convergence is achieved, additional mesh refinement has little effect on the outputs.

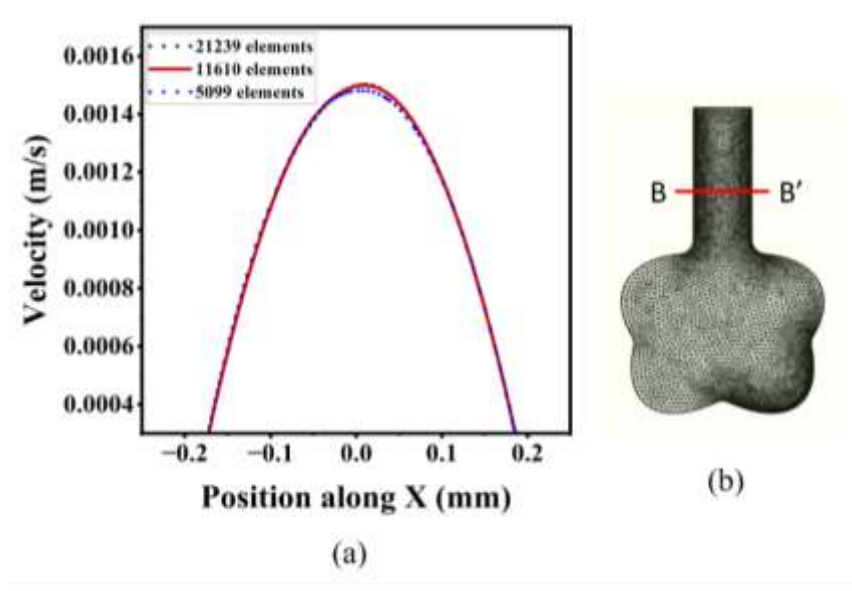


Figure 2: (a) Grid sensitivity test of airflow velocity and (b) Current mesh design

It is possible to read the model and its output without taking the mesh into account. In this investigation, a mesh element with maximum and lowest edge sizes of 0.14 mm and 0.000628 mm, respectively, was used to calculate the velocity magnitude in the duct model at time t=0s, 1.5s, 3s, 4.5s (See the Figure 2a). The elements of meshes were expected to expand at 1.3 times the rate of curvature, with a correction factor of 0.3. Three non-uniform grid sizes were investigated to verify grid independence. The minor modification was discovered for 11610 elements in total, which was chosen for finding the accurate answer in the current

case. Figure 2b also displays the current airflow velocity mesh structure.

Model validation is an essential part of the solution approach. For validating the accuracy of the solution approach, the numerical results were validated for fluid flow past in a 2D channel air flow velocity at time $t=0s,\ 1.5s,\ 3s,\ 4.5s$ and are compared with former published study of Qi, S., Zhang, B., Teng et al[41]. Figure 3 shows that our present study is in good agreement with the previous study of Qi, S., Zhang, B., Teng et al[41].

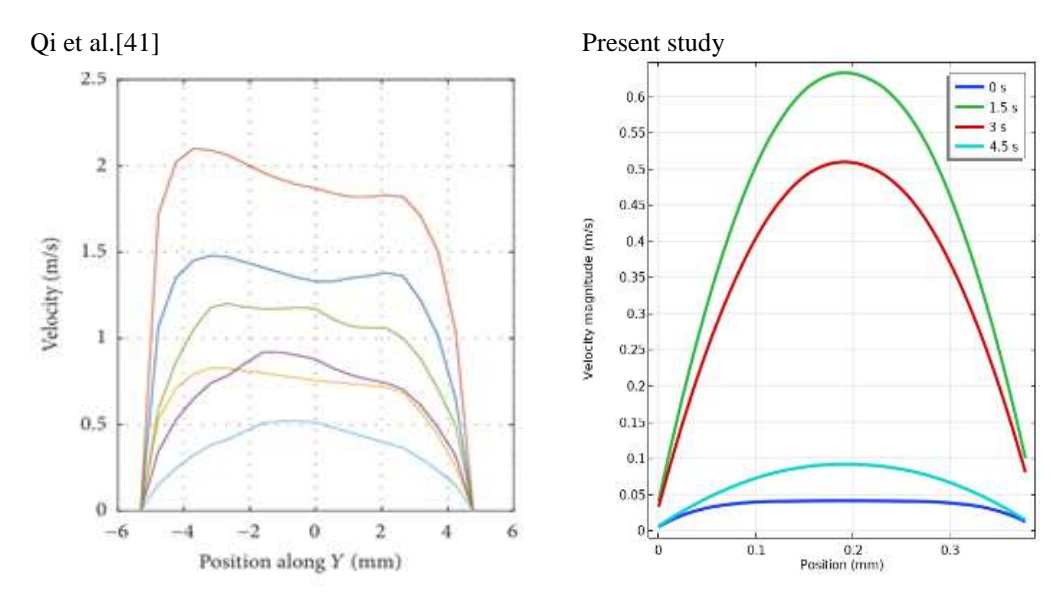


Figure 3: The validation of simulated air flow velocity for the time t = 0s, 1.5s, 3s, 4.5s

Result and discussions

During inhalation, air flows from the bronchioles into the alveolar sac. The velocity of air entering the alveolar sac decreases as it spreads out to fill the numerous alveoli. This decrease in velocity occurs because the cross-sectional area increases significantly as air moves from the bronchioles into the alveoli in the case of emphysema.

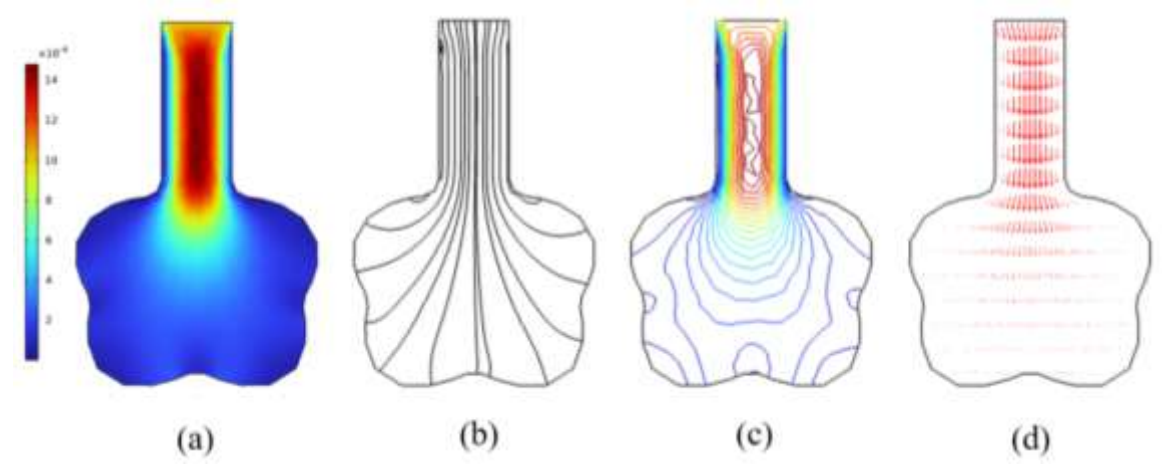


Figure 4: (a) surface, (b) streamline, (c) contour, and (d) arrow line of velocity profile

The flow within the alveoli is generally laminar rather than turbulent, particularly in healthy lungs [42]. Laminar flow means that air moves in smooth, orderly layers, which is ideal for efficient gas exchange. From figure 4 we can see that the largest velocity occurs in the duct which is 1.4 mm/s and the velocity decreases in the alveolar sac. near the wall it is almost zero according to no slip boundary condition.

Within the alveolar sac, air velocity is relatively low due to the large surface area provided by the effect of emphysema the inter alveolar walls have been collapse. The airflow is primarily driven by the pressure gradient established by the contraction of respiratory muscles. As air moves into the sac, it distributes more evenly among the alveoli, leading to a more uniform velocity profile. Figure 5 shows the highest velocity at BB' in the duct then the velocity decreases at CC'. in the alveolar space it becomes 1.2 and 0.45 at CC' and DD' respectively. At EE', we get flat curve with low skewness of velocity 0.33mm/s. The computational fluid dynamics (CFD) analysis the airflow patterns within the alveolar sac. Streamlines often show a more erratic flow pattern compared to larger, more straight segments of the air way. Velocity vectors are parabolic due to no slip boundary conditions.

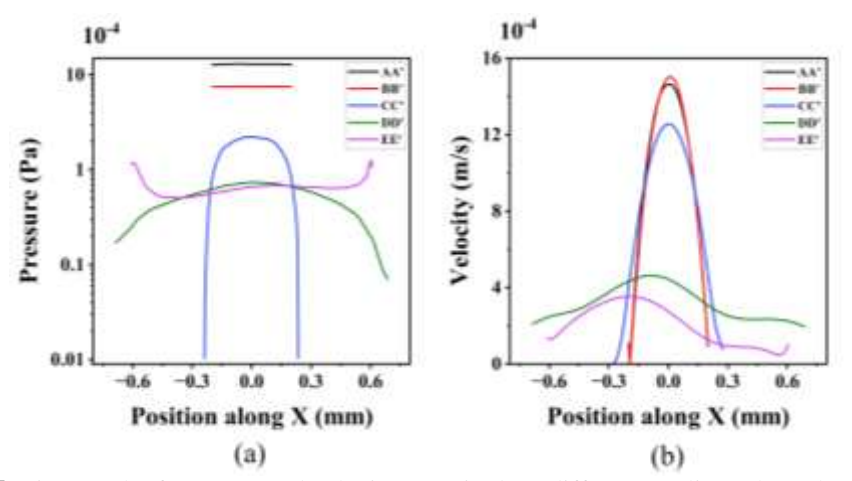


Figure 5: Line graph of pressure and velocity magnitude at different cut lines along the arc length

Pressure Distribution: In the case of Emphysema the pressure inside the alveolar sac is slightly lower than atmospheric pressure due to the expansion of the thoracic cavity. This pressure gradient drives air into the alveoli. Once air enters the alveolar sac, the pressure in the sac tends to equalize among the individual alveoli. This is due to the interconnected nature of the alveolar ducts and the alveoli themselves. Therefore, there is minimal pressure variation within the sac, as the air seeks to distribute evenly to equalize pressure [43 - 44].

The surface tension of the fluid lining the alveoli affects the local pressure. Surfactant reduces surface tension, preventing alveolar collapse and ensuring that pressure is more uniformly distributed. Without adequate surfactant, surface tension could cause variations in pressure within the sac, potentially leading to areas of higher pressure and increased risk of collapse [45 - 46]. The pressure distribution within the alveolar sac is relatively uniform, but slight gradients can be observed. Pressure differences drive the airflow, and these gradients influence how air and particles distribute across the sac. From figure 6, we can observe that highest pressure occurs in the alveolar duct.

Deposition Patterns: The CFD analysis provides detailed maps of particle deposition within the alveolar

sac for emphysema. Particles tend to deposit in regions of lower airflow velocity, where the flow is more stagnant. Deposition is often higher in the regions where the flow has been redirected or slowed due to the complex geometry of the alveoli.Smaller particles, particularly those in the nano to micrometer range, can be seen to penetrate deeper into the alveoli. Larger particles, due to inertial impaction, are more likely to be trapped in the upper regions of the alveolar sac or in the airways leading to the alveoli. The complexity of the alveolar sac's geometry significantly affects both airflow and particle deposition [47]. Irregularities or variations in the shape and size of alveoli create regions with different airflow characteristics, influencing where particles are most likely to deposit. The CFD analysis of airflow and particle deposition in an alveolar sac provides critical insights into how air moves and how particles are distributed within the lungs. These findings have significant implications for respiratory health, the design of inhalable medications, and understanding the effects of environmental pollutants. For COPD patient the structure of the alveolar sac changes due to the collapse or destruction of the alveolar wall which impact the deposition of the particle in the alveolar sac. Large space with no alveolar septa can change the deposition fraction.

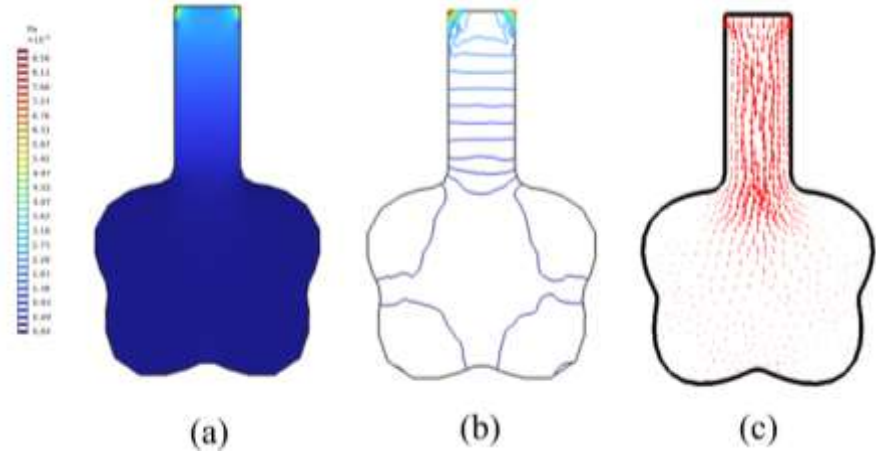


Figure 6: (a) Surface, (b) contour, and (c) arrow line of pressure profile

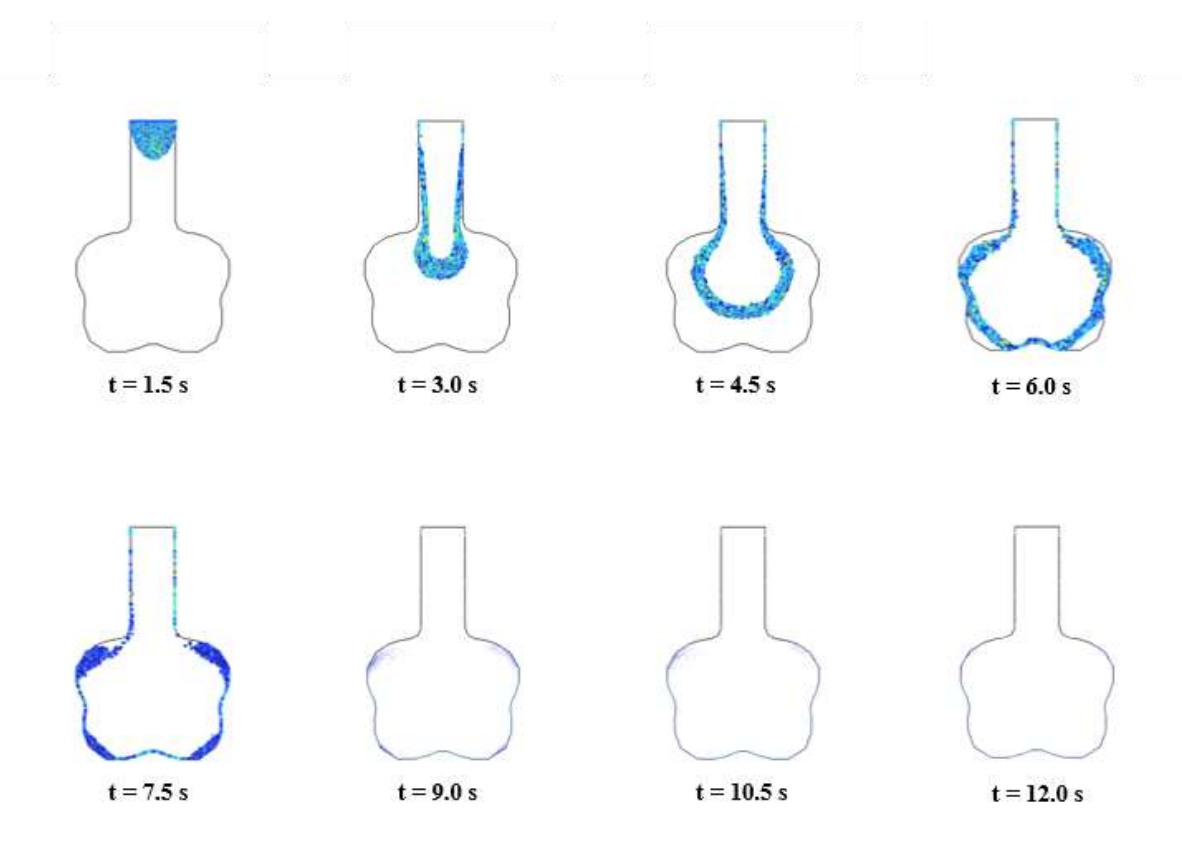


Figure 7: Particle trajectories at different time steps

Particle trajectories in the alveolar sacks are shown in the Figure 7. Instantaneous snapshots are shown in different time intervals. At the beginning of the inspiration particle were inhaled in the geometry from 0s to 1s. According to the inhalation flow rate particle showed parabolic shape at the alveolar duct and then became semi-circular through the alveolar space. At the end of the first inspiration cycle particle reach half way of the airspace. Most of the particles are deposited in the alveolar sacks due to drag force and gravitational sedimentation. Particles with a diameter of 200 nm deposit in a specific pattern on the surface, as shown in Figure 7. Particles primarily settled on the ground suggesting that gravitational sedimentation remains the dominant deposition mechanism. Figure 7 shows the particle deposition pattern when it occurs on the oscillating walls of the alveoli, indicating that particle deposition is not restricted to a single surface but can occur anywhere within the range. Considering the two lateral alveoli, no particles were observed on the distal walls, indicating a limited contribution from convective deposition. It took about 24 seconds to start deposition in the static model, which was dictated by the alveolar size over particle settling velocity; while in the dynamic model, deposition started almost immediately after particles enter the alveoli. Furthermore, once the deposition started, it took only a short period time for the deposition to complete in the static model; in contrast, the deposition in the dynamic model took about three cycles to complete in the upper alveolus and more than four cycles in the lower and lateral alveoli. Further, a multistage staggering profile of the deposition fraction (DF) versus time was observed in

each alveolus of the dynamic model. It is noted that, in this study, a particle bolus was inhaled into the geometry at the start of the inhalation. Particle boluses inhaled at later instances will have lower deposition rates, time required for deposition was very different between different particle sizes. It took around 45 s for 0.5 µm particles to complete the deposition, while it took 12 s for 1 µm particles, 4 s for 2 µm particles, and 2 s for 3 µm particles [48]. Deposition fraction decreases due to the increasing particle settling velocity, which is proportional to the square of the particle diameter Furthermore, deposition of 0.5 µm particles started 21 s after administration in the two lateral alveoli and 33 s in the lower alveoli. By contrast, much shorter periods of time were needed for larger particles. For instance, it took 1 s for 2 µm particles to start deposition in the lateral alveoli and 1.5 s in the lower alveoli [53]. The deposition fraction in emphysema model are shown in Figure 8.

Particle deposition in different regions of the alveolar sac model as a function of time is shown in Figure 7 for 200 nm aerosol particle the respiration rate is 20 BPM (t =3 s). It is noted that aerosols are released from the inlet plane of the duct at the beginning of the inhalation. This practice was to ensure that the same number of particles would be tracked; otherwise, a varying number of particles could be instantly lost due to random motion during their release. Only particles within the computational domain could be tracked. Considering 200-nm aerosol particles completed their deposition on the duct almost instantly, even though there was slightly more deposition at the beginning of the second inhalation cycle. At 7.5s particles are started

to deposit in the alveolar wall. After three cycles (t = 9s) almost all the particles are deposited inside the

region.

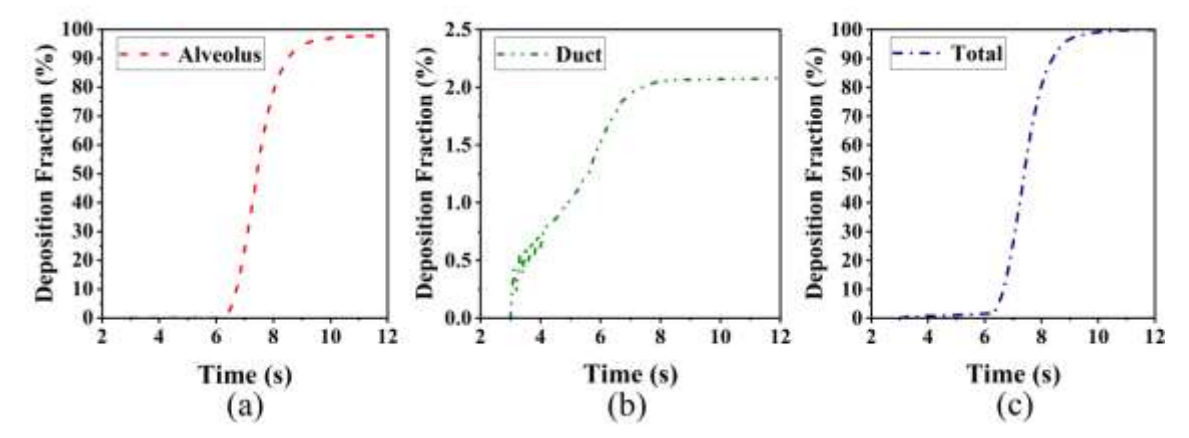


Figure 8: Particle deposition fraction in (a) alveolar space, (b) duct, and (c) total sac

As expected, a higher fraction of particles deposited in the alveolus had the highest deposition fraction or DF (98%). In contrast to the quick deposition in the duct, deposition in the sac (alveolus) was more gradual and took even longer time to complete in larger domain. Besides, more particles deposited in larger spheres as opposed to less deposition in larger ducts. However, the DF increase with the sphere volume is not linear with the alveolus size, with a larger increase in small alveoli, while a very small increase in large alveoli [49-51] . This nonlinear DF variation with geometrical scale raised a question that could not be explained by considering any individual factors separately, such as gravitational sedimentation, diffusion, or advection. Rather, an understanding of the relationship (or rival) among the above three mechanisms is needed. Overall, more particles deposit in the bottom of the sac with either increasing particle size or geometrical scale. A highly concentrated particle deposition is observed at the interconnected alveolus. A highly dispersed distribution throughout the alveolar space in the model for 200 nm aerosols is also viewed. However, deposition in the alveoli [52] exhibits a clear response geometrical scale. which monotonously with increasing alveolar size (Figure 8). Deposition fraction increases in emphysema model in compare to other normal model from previous study [14].

Conclusion

In conclusion, the study involves a 2D model of alveolar sac which has been deformed under emphysematous condition. This study provides a comprehensive analysis of airflow dynamics and particle behavior within the alveolar sac under the conditions. Computational Fluid Dynamics (CFD) modeling revealed that structural degradation associated with emphysema—such as alveolar wall destruction and airspace enlargement—substantially alters local airflow patterns and particle transport. Maximum velocity magnitude has been found in the duct which is 0.0015mm/s. These morphological changes lead to airflow heterogeneity, increased

particle deposition up-to 98% in peripheral regions, and impaired clearance mechanisms. The findings underscore the critical role of microstructural alterations in influencing respiratory function and highlight the importance of considering disease-specific airflow patterns in the design of aerosol-based therapies. Ultimately, this work contributes to a deeper understanding of pulmonary mechanics in emphysema and offers a foundation for future research into personalized treatment strategies.

Acknowledgments

All authors would like to state their gratefulness to the Department of Arts and Sciences, Ahsanullah University of Science and Technology (AUST), Dhaka-1208 and Department of Applied Mathematics, University of Dhaka, Dhaka-1000, for endowing with computing facility during this research work.

Funding Statement

The authors received no specific funding for this study.

CRediT authorship contribution statement

N. T. Mim: Code Validation, Data collection, Investigation, Analysis and interpretation of results, Writing- first draft; Muhammad Sajjad Hossain: Study conception and design, Writing-first and original draft, Data collection, Resources, Methodology, Visualization, Analysis and interpretation of results, Supervision, Project Administration, Writing review and editing; M. S. I. Mallik: Visualization, Formal Analysis, data collection, Resources, Writing review and editing; M. Masum Billah: Methodology, Investigation, data collection, Resources, Writing review and editing; S. M. C. Hossain: Code Validation, Visualization, Resources, Writing review and editing. All authors reviewed the results and approved the final version of the manuscript.

Conflicts of Interest

The authors declare that they have no conflicts of interest to report regarding the present study.

Availability of Data and Materials

Ethics Approval

All authors declare that data availability is not applicable to this article.

Not applicable.

Nomenclatures

Symbol	Description	Units
u	Airflow velocity vector	m/s
p	Pressure	Pa
ρ	Air density	kg/m³
$\boldsymbol{\rho}_p$	Particle density	kg/m³
μ	Dynamic viscosity of air	$Pa \cdot s$
d_p	Particle diameter	μm
v_p	Particle velocity vector	m/s
m_p	Particle mass	kg
τ_p	Particle relaxation time	S
Re	Reynolds number (based on alveolar scale)	_
g	Gravitational acceleration	m/s^2
F_d	Drag force on particle	N
t	Time	S
Q	Volumetric flow rate	m^3/s

References

- [1] Brackenbury, J. (1981) .Airflow and respired gases within the lung-air-sac system of birds. Comparative Biochemistry and Physiology Part A: Physiology, 68(1), 1–8. https://doi.org/10. 1016/0300-9629(81)90309-1.
- [2] Cinkotai, F. F. (1974). Fluid flow in a model alveolar sac. Journal of applied physiology, 37(2), 249–251. https://doi.org/10.1152/jappl. 1974.37.2.249.
- [3] Dong, J., Yang, Y., and Zhu, Y. (2022). Recent advances in the understanding of alveolar flow. Biomicrofluidics, 16 (2):021502. doi: 10.1063/5.0084415.
- [4] Kim, J., Heise, R. L., Reynolds, A. M. and Pidaparti, R. M. (2017). Aging effects on airflow dynamics and lung function in human bronchioles. PloS one, 12(8):e0183654. doi: 10.1371/journal.pone.0183654.
- [5] Kumar, H., Tawhai, M. H., Hoffman, E. A. and Lin, C.-L. (2009). The effects of geometry on airflow in the acinar region of the human lung. Journal of Biomechanics, 42 (11), 1635–1642. doi:
 - https://doi.org/10.1016/j.jbiomech.2009.04.046.
- [6] Li, P., Guo, W., Fan, J., Su, C., Zhao, X. and Xu, X. (2023). Fluid-structure interaction analysis of airflow, structural mechanics and aerosol dynamics in a four-generation acinar model. Journal of Aerosol Science, vol. 171 (106166). https://doi.org/10.1016/j.jaerosci.2023.106166.
- [7] Li, Z. and Kleinstreuer, C. (2011). Airflow analysis in the alveolar region using the lattice-Boltzmann method. Medical & biological engineering & computing, 49(4),441–451. doi: 10.1007/s11517-011-0743-1.
- [8] Ma. B. and Darquenne, C. (2011). Aerosol deposition characteristics in distal acinar airways

- under cyclic breathing conditions. Journal of Applied physiology, 110(5), 1271–1282. https://doi.org/10.1152/japplphysiol.00735.2010.
- [9] Weibel, E.R. (1963). Morphometry of the Human Lung. Springer Verlag and Academic Press, New York. http://dx.doi.org/10.1007/978-3-642-87553-3.
- [10] Sznitman, J. (2008). Respiratory flows in the pulmonary acinus and insights on the control of alveolar flows. ETH Zurich.
- [11] Sznitman, J., Sutter, R., Altorfer, D., Stampanoni, M., Rösgen, T. and Schittny, J. C. (2010). Visualization of respiratory flows from 3D reconstructed alveolar airspaces using X-ray tomographic microscopy. Journal of visualization, 13, 337–345. DOI 10.1007/s12650-010-0043-0.
- [12] Sera, T., Uesugi, K., Yagi, N., and Yokota, H.(2015). Numerical simulation of airflow and microparticle deposition in a synchrotron micro-CT-based pulmonary acinus model. Computer methods in biomechanics and biomedical engineering, 18(13),1427–1435. https://doi.org/10.1080/10255842.2014.915030
- [13] Reis, A. H., Miguel, A. F. and Aydin, M. (2004). Constructal theory of flow architecture of the lungs. Medical physics, 31(5), 1135–1140. DOI: 10.1118/1.1705443.
- [14] Xi, J., Talaat, M., Tanbour, H. and Talaat, K. (2018). Airflow and particle deposition in acinar models with interalveolar septal walls and different alveolar numbers. Computational and mathematical methods in medicine, 2018 (1):3649391. doi: 10.1155/2018/3649391.
- [15] Sul, B., Wallqvist, A., Morris, M. J., Reifman, J., & Samp; Rakesh, V. (2014). A computational study of the respiratory airflow characteristics in normal

- and obstructed human airways. Computers in biology and medicine, 52, 130-143.
- [16] Jr, E. M. H. and Robinson, R. J. (2010). Flow in a terminal alveolar sac model with expanding walls using computational fluid dynamics. Inhalation Toxicology,22 (8), 669–678.DOI: 10.3109/08958371003749939.
- [17] Nowak, N., Kakade, P. P. and Annapragada, A. V. (2003). Computational fluid dynamics simulation of airflow and aerosol deposition in human lungs. Annals of biomedical engineering, 31, 374–390. https://doi.org/10.1114/1.1560632.
- [18] Kumar, H. (2011). Study of airflow and particle transport in acinar airways of the human lung. Doctoral dissertation, The University of Iowa.
- [19] Byron, PR. (1986). Prediction of drug residence times in regions of the humanrespiratory-tract following aerosol inhalation. J Pharm Sci 75: 433–438.
- [20] Darquenne, C., Harrington, L., and Prisk, G. K. (2009). Alveolar duct expansion greatly enhances aerosol deposition: a three-dimensional computational fluid dynamics study. Philosophical Transactions of the Royal Soc iety A: Mathematical, Physical and Engineering Sciences, 367(1896), 2333-2346.
- [21] Hofemeier, P., and Sznitman, J. (2015). Revisiting pulmonary acinar particle transport: convection, sedimentation, diffusion, and their interplay. Journal of Applied Physiology, 118(11), 1375-1385.
- [22] Hofemeier, P., and Sznitman, J. (2016). The role of anisotropic expansion for pulmonary acinar aerosol deposition. Journal of biomechanics, 49(14), 3543-3548.
- [23] Hofemeier, P., and Sznitman, J. (2014). Role of alveolar topology on acinar flows and convective mixing. Journal of Biomechanical Engineering, 136(6), 061007.
- [24] Francis, I., and Saha, S. C. (2022). Surface tension effects on flow dynamics and alveolar mechanics in the acinar region of human lung. Heliyon, 8(10).
- [25] Kumar, H., Tawhai, M. H., Hoffman, E. A., and Lin, C. L. (2009). The effects of geometry on airflow in the acinar region of the human lung. Journal of biomechanics, 42(11), 1635-1642.
- [26] Nieman, G. F., and Habashi, N. M. (2024). Alveolar and Alveolar Duct (Acinar) Mechanics in the Normal Lung. In Applied Physiology to Reduce Ventilator Induced Lung Injury: Clinical Applications for the Acutely Injured Lung (pp. 37-54). Cham: Springer Nature Switzerland.
- [27] Dudurych, I., Muiser, S., McVeigh, N., Kerstjens, H. A., van den Berge, M., de Bruijne, M., and Vliegenthart, R. (2022). Bronchial wall parameters on CT in healthy never-smoking, smoking, COPD, and asthma populations: a systematic review and meta-analysis. European Radiology, 32(8), 5308-5318.

- [28] Eom, J. S., Lee, G., Lee, H. Y., Oh, J. Y., Woo, S. Y., Jeon, K., and Park, H. Y. (2013). The relationships between tracheal index and lung volume parameters in mild-to-moderate COPD. European Journal of Radiology, 82(12), e867-e872.
- [29] Wiebe, B. M., and Laursen, H. (1995). Human lung volume, alveolar surface area, and capillary length. Microscopy research and technique, 32(3), 255-262.
- [30] Jelic, T. M. (2019). Emphysema. In Update in Respiratory Diseases. IntechOpen.
- [31] Hogg, J., and Senior, R. (2002). Chronic obstructive pulmonary disease c 2: Pathology and biochemistry of emphysema. Thorax, 57(9), 830.
- [32] Hsia, C. C., Hyde, D. M., and Weibel, E. R. (2016). Lung structure and the intrinsic challenges of gas exchange. Comprehensive physiology, 6(2), 827.
- [33] Park, J. G., Aksamit, T. R., Swanson, K. L., and Thomas Jr, C. F. (2006). Pulmonary diseases. Mayo Clinic Internal Medicine Review, 7th ed. New York, NY: Informa Healthcare.
- [34] Berthiaume, Y., Folkesson, H. G., and Matthay, M. A. (2002). Invited review: alveolar edema fluid clearance in the injured lung. Journal of Applied Physiology, 93(6), 2207-2213.
- [35] Yager, D., Feldman, H., and Fung, YC.(1992). Microscopic vs. macroscopic defor-mation of the pulmonary alveolar duct. J. Appl Physiol 72: 1348 –1354.
- [36] Chen, L., and Zhao, X. (2019). Characterization of air flow and lung function in the pulmonary acinus by fluid-structure interaction in idiopathic interstitial pneumonias. Plos one, 14(3), e0214441.
- [37] Dechaumphai, P., Triputtarat, J., and Sikkhabandit, S. (1998). A Finite Element Method for Viscous in Compressible Flow Analysis. Science & Technology Asia, 60-68.
- [38] Reusken, A. (2025). Analysis of the Taylor-Hood surface finite element method for the surface Stokes equation. Mathematics of Computation, 94(354), 1701-1719.
- [39] Reddy, J. N. (1993). An introduction to the finite element method. New York, 27(14).
- [40] Querin, O., Nicolás, M. V., and Gordoa C. A. (2017). Discrete Method of Structural Optimization, 2017, 27-46. DOI: 10.1016/B978-0-08-100916-1.00003-9
- [41] Qi, S., Zhang, B., Teng, Y., Li, J., Yue, Y., Kang, Y., and Qian, W. (2017). Transient dynamics simulation of airflow in a CT-scanned human airway tree: more or fewer terminal bronchi? Computational and mathematical methods in medicine, 2017(1), 1969023.
- [42] Tsuda, A., Henry, FS., and Butler, JP.(1995). Chaotic mixing of alveolated duct flowin rhythmically expanding pulmonary acinus. J Appl Physiol 79: 1055–1063.
- [43] Park, SS., and Wexler, AS.(2007). Particle deposition in the pulmonary region of thehuman lung: a semi-empirical model of single breath

- transport anddeposition. J Aerosol Sci 38: 228 245.
- [44] DeGroot, C. T. and Straatman, A. G. (2016). A conjugate fluid–porous approach for simulating airflow in realistic geometric representations of the human respiratory system. Journal of Biomechanical Engineering, 138(3):034501.
- [45] Saray, M. A. E., Saidi, M. S., and Ahmadi, G. (2017). Airflow patterns in a 3D model of the human acinus. Scientia Iranica, 24(5), 2379 2386.
- [46] Farmer, C. and Sanders, K. (2010). Unidirectional airflow in the lungs of alligators. Science, vol. 327(5963), 338–340.
- [47] Sznitman, J., Heimsch, F., Heimsch, T., Rusch, D. and Rösgen, T. (2007). Three-dimensional convective alveolar flow induced by rhythmic breathing motion of the pulmonary acinus. J Biomech Eng., 129(5):658-65. doi: 10.1115/1.2768109.
- [48] Sznitman, J., Heimsch, T., Wildhaber, J. H., Tsuda, A. and Rösgen, T. (2009). Respiratory flow phenomena and gravitational deposition in a three-dimensional space-filling model of the pulmonary acinar tree. J Biomech Eng., 131(3):031010. doi: 10.1115/1.3049481. 2009.
- [49] Talaat, M., Si, X. A., Tanbour, H. and Xi, J. (2019) "Numerical studies of nanoparticle transport and deposition in terminal alveolar models with varying complexities," Med One, 4:4:e190018.
- [50] Miguel, A. F. (2011). Lungs as a natural porous media: architecture, airflow characteristics and transport of suspended particles. In: Delgado, J. (eds) Heat and mass transfer in porous media: Springer, 2011, 13, 115–137. https://doi.org/10.1007/978-3-642-21966-5_5.
- [51] Monjezi, M. and Saidi, M. (2016). Fluid-structure interaction analysis of air flow in pulmonary alveoli during normal breathing in healthy humans. Scientia Iranica, 23(4),1826–1836.
- [52] Sverdlova, N., Lambertz, M., Witzel, U. and Perry, S. (2012). Boundary Conditions for Heat Transfer and Evaporative Cooling in the Trachea and Air Sac System. PLoS One. 2012;7(9):e45315.

doi: 10.1371/journal.pone.0045315.